(Received 27 August 2024, Accepted 14 October 2024, Scheduled 22 October 2024)

Compact 8-Port MIMO Antenna for Hot-Spot Applications Based on Embedded Double-Negative Metamaterial Split Ring Resonators

Jose Alfredo Tirado-Mendez[1, 2, *], Arturo Rangel-Merino[1], and Luis Vasquez-Toledo[3]

[1] *SEPI-Electrical Engineering, ESIME Zacatenco, Instituto Politécnico Nacional*
Av. IPN S/N, San Pedro Zacatenco, Mexico City 07738, Mexico
[2] *Telecommunications Section, CINVESTAV-IPN*
Av. IPN 2508, San Pedro Zacatenco, Gustavo A. Madero, Mexico City 07360, Mexico
[3] *Electrical Engineering Department, UAM-Iztapalapa*
Av. San Rafael Atlixco 186, Leyes de Reforma 1ra Secc, Iztapalapa, Mexico City 09340, Mexico

ABSTRACT: This article proposes an 8-port MIMO antenna based on double-negative metamaterial Split Ring Resonators (SRRs) for three-dimensional (3D) non-planar applications, such as hotspots. The antenna features eight radiators arranged orthogonally to each other, placed in two perpendicular planes, operating at 3.5 GHz. Each resonator incorporates six embedded SRRs to enhance the metamaterial behavior, achieving a 40% size reduction compared to a conventional disc monopole at the same frequency. Simulated and measured results demonstrate excellent performance for MIMO applications, with Envelope Correlation Coefficient (*ECC*) values below 0.001 and Diversity Gain (*DG*) around 20 dB. The Total Active Reflection Coefficient (*TARC*) bandwidth is approximately 930 MHz at the -10 dB threshold. The S-parameters indicate excellent electromagnetic isolation between radiators exceeding 20 dB, and a very low cross-polarization level below -30 dB. However, the main limitation of this design is a reduction in gain, an expected result.

1. INTRODUCTION

Multiple-Input Multiple-Output (MIMO) antennas play a crucial role in the performance of modern and near-future communication systems. These antennas consist of multiple radiators placed in close proximity for personal devices. However, for optimal performance, these radiators must simultaneously achieve high diversity and multiplexity gain. On the other hand, miniaturization of radiator elements is a key requirement for modern handsets and hotspot architectures. Several techniques have been employed to reduce the size of passive circuits, including antennas. These techniques encompass Defected Microstrip Structures [1], acoustic excitation [2], stub loading [3], fractal geometries [4], metamaterials [5], and others.

In the case of MIMO antennas, especially those designed for handsets, the close spacing among radiators leads to high mutual electromagnetic coupling, which can degrade the performance of the antenna array. Several architectures have been proposed to address this challenge [6]. Therefore, while miniaturization of MIMO arrays is essential for mobile communications, a trade-off between element size and radiator spacing is necessary to overcome the detrimental effects of electromagnetic coupling.

On the one hand, as mentioned before, metamaterial structures can be a useful technique to reduce the size of a passive circuit, in this case, an antenna. However, metamaterial surfaces can also provide other advantages when being employed in these devices, such as increasing the gain [7]. In this article, the metamaterial surface, implemented using embedded Split Ring Resonators (SRRs), is used to reduce the size of the antenna without compromising its bandwidth and impedance matching performance.

Several proposals for eight-element MIMO antennas in a 2D configuration have been reported [8–13]. While some of these designs offer the advantage of simplicity by using resonant slots, others present challenges in design and geometry. Other configurations utilize eight resonators in a 3D structure, as exemplified by the works in [14–16]. The antenna in [14] features a 3D arrangement of eight elements with both symmetric and non-symmetric configurations on an octagonal polystyrene structure, targeting system-in-package applications and wireless personal networks. This antenna also leverages a metamaterial configuration to improve radiator performance. In [15], although the authors claim that the proposed antenna is intended for handsets, caution is necessary due to the array structure. The radiators are perpendicular to the main plane, indicating a 3D structure. Finally, the authors in [16] present a configuration where the radiators are placed on two perpendicular planes, resulting in orthogonal antennas.

In this article, an eight-element MIMO antenna is presented, configured in two perpendicular planes similar to the one described in [16]. The unit radiator is designed as a monopole with embedded SRRs to reduce the overall antenna size com-

* Corresponding author: Jose Alfredo Tirado-Mendez (jtiradom@ipn.mx).

pared to a conventional disc monopole. Each plane houses four orthogonally placed radiators. The design, simulations, and results are presented in the following sections.

2. ANTENNA DESIGN AND SIMULATION RESULTS

The design is based on a configuration of embedded split-ring resonators (SRRs). It has been demonstrated that a set of two SRRs [17] exhibit metamaterial behavior, and thus, by including more embedded rings, the metamaterial behavior is enhanced. As a result of the increased metamaterial effect, a higher slow-wave factor is obtained, indicating a longer electrical length for a smaller metallic structure. With this result, a more compact resonant structure can be obtained, but it resonates at a lower frequency. Additionally, by using a larger set of embedded rings, a metamaterial effect is achieved over a wider bandwidth than that when only two rings are employed. The proposed antenna, based on a set of embedded SRRs, is presented in Figure 1, designed on a Duroid substrate with a permittivity of 4.5 and a thickness of 0.787 mm. The radiator is fed by a microstrip line, where the ground plane, on the back side of the substrate, is represented in black, and the SRR radiator is colored in gray, on the front side of the substrate. The initial dimensions are selected such that the length of the radiator, from the ground plane, is at least 30% shorter than a quarter-wave monopole resonating at the same frequency. The selected band is 3.5 GHz due to its interest in 5G telephony applications. The optimization of the dimensions is achieved through a parametrization process using the Ansys Electronics simulation software, considering a trade-off between bandwidth, compact size, and port matching below -10 dB.

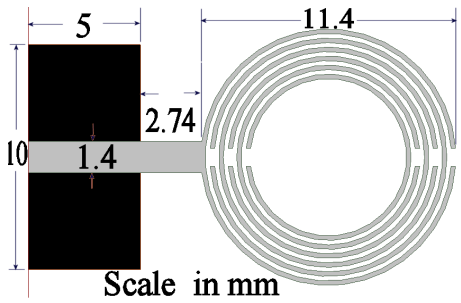

FIGURE 1. Metamaterial structure antenna with SRRs.

The widths and separations between the rings are set to 0.2 mm. The antenna is designed to resonate at 3.5 GHz. Compared to a conventional quarter-wavelength ($\lambda/4$) radiator, the proposed antenna is nearly 34% shorter after dimension optimization.

The metamaterial behavior is presented in Figure 2. Equations (1) to (4) in [18] detail the calculation of the real and imaginary parts of the permittivity and permeability. Following the procedure outlined in [18], the permeability (μ) is obtained by $\mu = nz$, and the permittivity (ε) is obtained by the expression $\varepsilon = n/z$, where n is the refractive index, and z is the impedance. The refractive index and impedance are closely related to the S-parameters as:

$$z = \pm\sqrt{\frac{(1+S_{11})^2 - S_{21}^2}{(1-S_{11})^2 - S_{21}^2}} \tag{1}$$

$$n = \pm\frac{1}{jL}\left(\frac{c}{\omega}\right)\cosh^{-1}\left(\frac{1-S_{11}^2+S_{21}^2}{2S_{21}}\right) \tag{2}$$

The signs in (1) and (2) are determined by:

$$z' \geq 0 \tag{3}$$

$$n'' \geq 0 \tag{4}$$

where $(\cdot)'$ and $(\cdot)''$ denote the real part and imaginary part operators, respectively.

Simulating the structure shown in Figure 1 as a two-port configuration, where the second port is considered as a part of the radiation environment in front of the rings, as depicted in Figure 2(a), and employing (1) to (4), the real and imaginary parts of the permeability and permittivity are presented in Figure 2.

As observed in Figure 2, the real parts of both the permittivity and permeability exhibit negative values at the design frequency of 3.5 GHz, signifying a double-negative metamaterial.

3. 8-PORT MIMO ARRAY CONFIGURATION

Leveraging this property, the antenna array is designed on two orthogonal planes, each one placing four elements in axial symmetry. The elements are positioned perpendicular to each other on each orthogonal plane to enhance electromagnetic isolation between radiators, as shown in Figure 3. Figure 3(a) shows the arrangement of the radiators in one plane, depicting the axial symmetry, and Figure 3(b) presents the isometric view of the 8 elements in both orthogonal planes. The separation among radiators was obtained considering the higher electromagnetic isolation.

Each planar element measures 45 mm by 45 mm. The center-to-center separation between the radiators is 26.3 mm. Antennas 1 to 4 are located on the horizontal substrate and are colored red for distinction. Antennas 5 to 8 are positioned on the vertical substrate and are shown in a dark color for clarity. The simulated S-parameters of the proposed antenna array are presented in Figure 4. Because of the axial symmetry, the results are limited to the interaction of the radiators with Antenna 1, since other combinations result in similar behavior.

The simulated S-parameters in Figure 4(a) indicate that all radiators exhibit a resonance around 3.3 GHz, but still coupling at 3.5 GHz. Conversely, the electromagnetic isolation between elements of the array is below -20 dB, reaching values around -30 dB at the desired frequency. An exception is the interaction between Antenna 1 and Antenna 8, where the S_{18} parameter remains around -20 dB. Nevertheless, the overall isolation is sufficient for MIMO applications.

Next, the results obtained from the simulation process are used to evaluate metrics relevant to MIMO performance. The envelope correlation coefficient (ECC) is calculated for each pair of antennas. Due to the axial symmetry of the array, only the ECC between the first antenna and the other antennas is

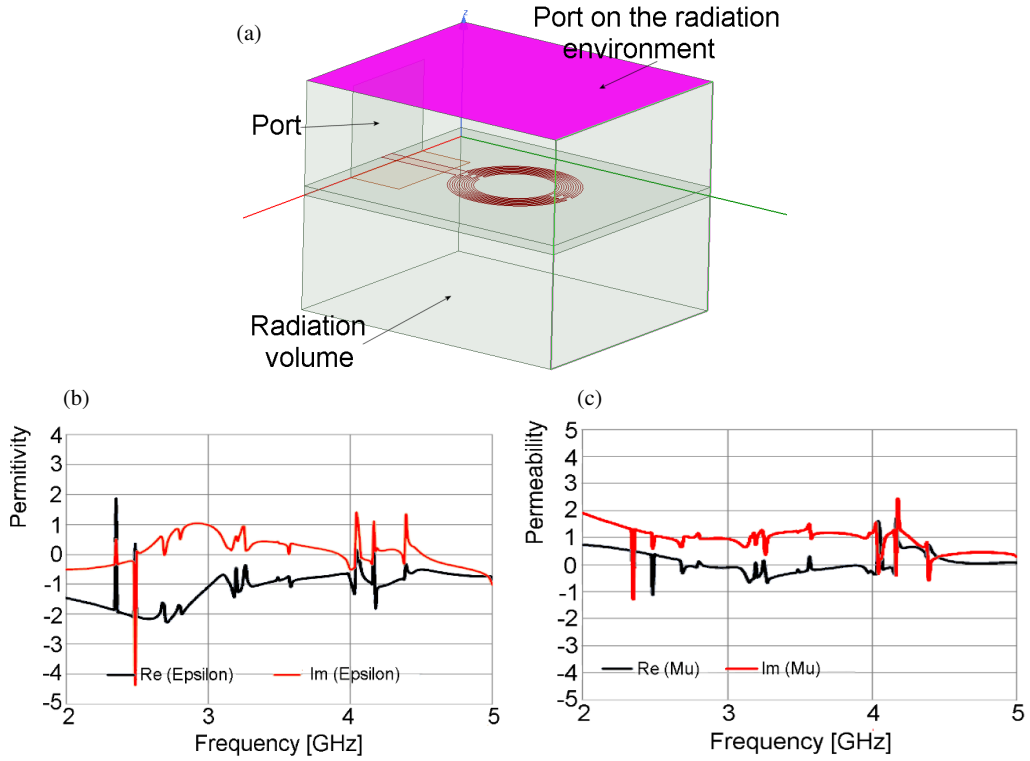

FIGURE 2. (a) Two port simulation model. (b) Real and imaginary parts of the permittivity. (c) Real and imaginary parts of the permeability.

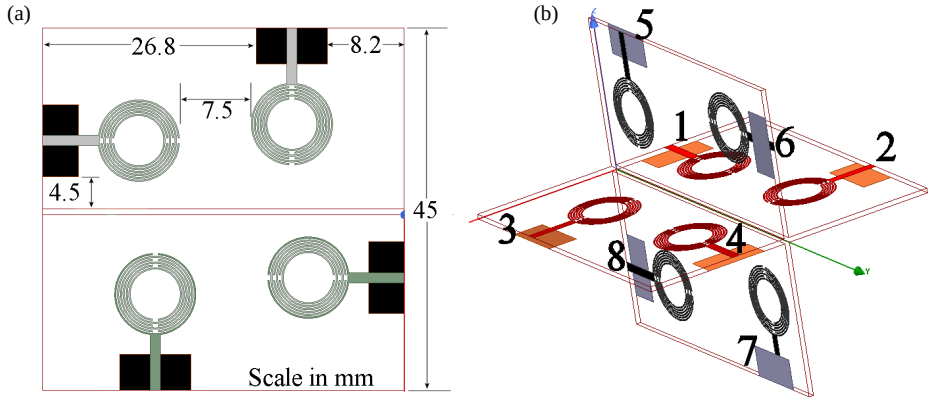

FIGURE 3. (a) One plane view. (b) Isometric view of the 8-port MIMO antenna.

presented in Figure 5. It can be inferred that the *ECC* values for other pairings of antennas will exhibit similar characteristics.

The *ECC* is given as a function of the *S*-parameters as (5):

$$ECC = \frac{\left|S_{11}^{*}S_{12} + S_{21}^{*}S_{22}\right|^{2}}{\left(1 - \left|S_{11}\right|^{2} - \left|S_{21}\right|^{2}\right)\left(1 - \left|S_{22}\right|^{2} - \left|S_{12}\right|^{2}\right)} \quad (5)$$

The results of the envelope correlation coefficient (*ECC*) for other antenna pairs exhibit high similarity to the curves presented in Figure 5. To enhance clarity and avoid redundancy, additional curves have not been included.

The analysis of Figure 5 reveals that the value of this parameter at the desired frequency is very small, reaching values lower than 0.0012 at 3.5 GHz, and below 0.012 from 3 GHz to 4 GHz. This indicates a very low level of correlation between the electric fields of the radiators.

Another metric employed to assess the performance of MIMO antennas is diversity gain. This parameter can be calculated using Equation (6).

$$DG = 10\sqrt{1 - (ECC)^{2}} \quad (6)$$

Table 1 shows the behavior of the *DG* for the antennas related to Antenna 1 at 3.5 GHz.

An analysis of Table 1 reveals that the antenna exhibits significant improvement in diversity gain, achieving near-maximum values of 20 dB for all radiator combinations.

On the other hand, the Total Active Reflection Coefficient (*TARC*) is then evaluated to assess the system bandwidth and

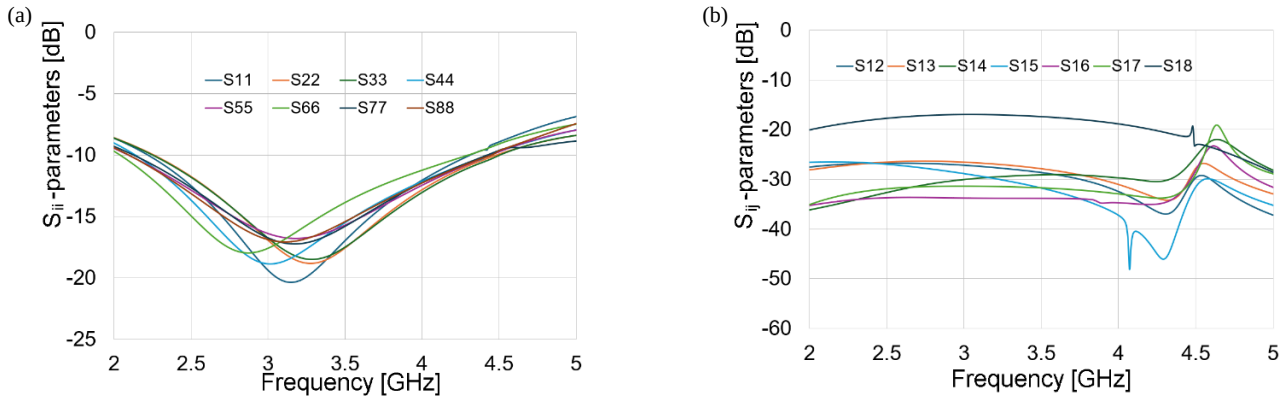

FIGURE 4. Simulated S-parameters of the proposed MIMO antenna. (a) Return loss of each antenna. (b) Isolation between Antenna 1 and the remaining resonators.

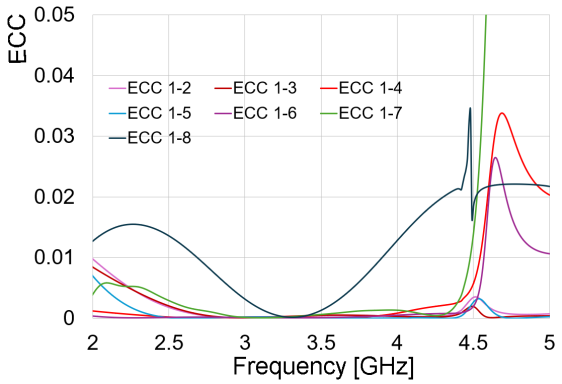

FIGURE 5. Envelope Correlation Coefficient relating Antenna 1 to i with $i = 2$ to 8.

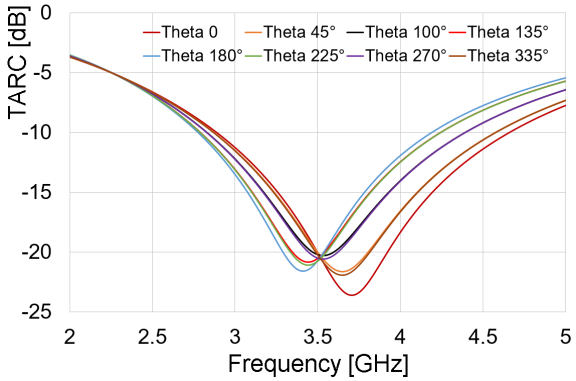

FIGURE 6. *TARC* of the proposed antenna varying θ_1.

TABLE 1. Diversity gain at 3.5 GHz.

Antenna 1 to Antenna n	DG [dB]
$n = 2$	19.99
$n = 3$	19.99
$n = 4$	20
$n = 5$	20
$n = 6$	20
$n = 7$	20
$n = 8$	19.99

overall functionality of the antenna array. As described in Equation (7), the *TARC* for N antennas is expressed as:

$$TARC = N^{-0.5}\sqrt{\sum_{i=1}^{N}\left|\sum_{k=1}^{N} S_{ik}e^{j\theta_{k-1}}\right|^2} \qquad (7)$$

Considering the large number of antennas and the inherent complexity of analyzing all possible phase combinations given in (7) by θ_{k-1}, the investigation focuses on a simplified case where all phases (θ_1 to θ_7) are initially set to 0°. Subsequently, θ_1 is varied to evaluate the impact on the *TARC*. The results of this analysis are presented in Figure 6.

This analysis aims to demonstrate that the behavior of the curves as a whole, for various incoming phases of the random signals at each radiator, maintains the system bandwidth below −10 dB. As observed, all curves for different phases exhibit a similar pattern, and the system bandwidth ranges from 2.9 GHz to 4.15 GHz, satisfying the requirement for the operating frequency of 3.5 GHz.

Following these results, the prototype was constructed, and the measurements will be presented in the subsequent section.

4. MEASURED RESULTS

The prototype was built, and its photograph is presented in Figure 7. The measured S_{ii} parameters, characterizing the re-

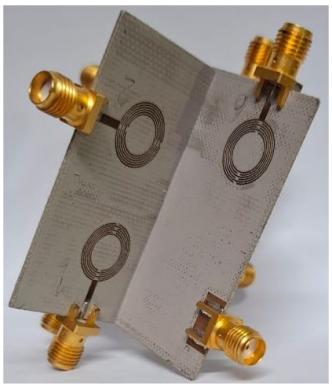

FIGURE 7. 8-port MIMO antenna prototype.

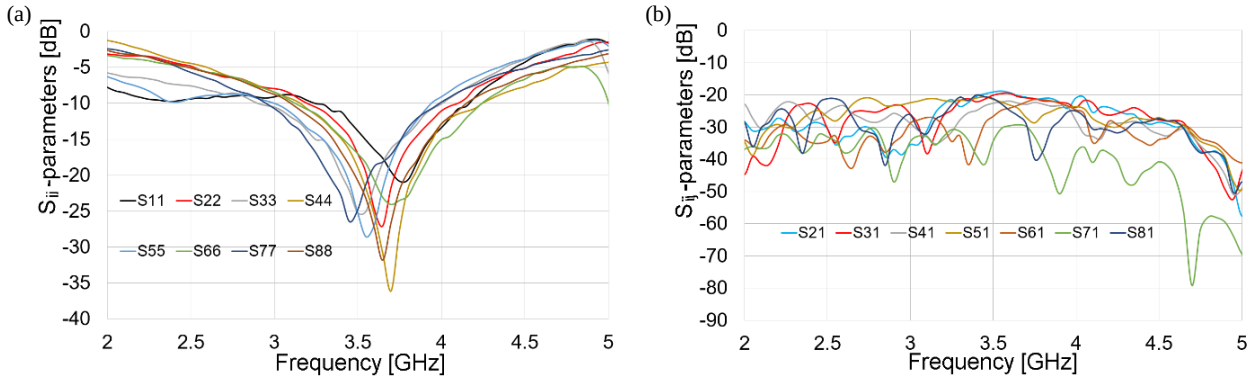

FIGURE 8. Measured S-parameters of the 8-port MIMO prototype. (a) S_{ii}, (b) S_{ij}.

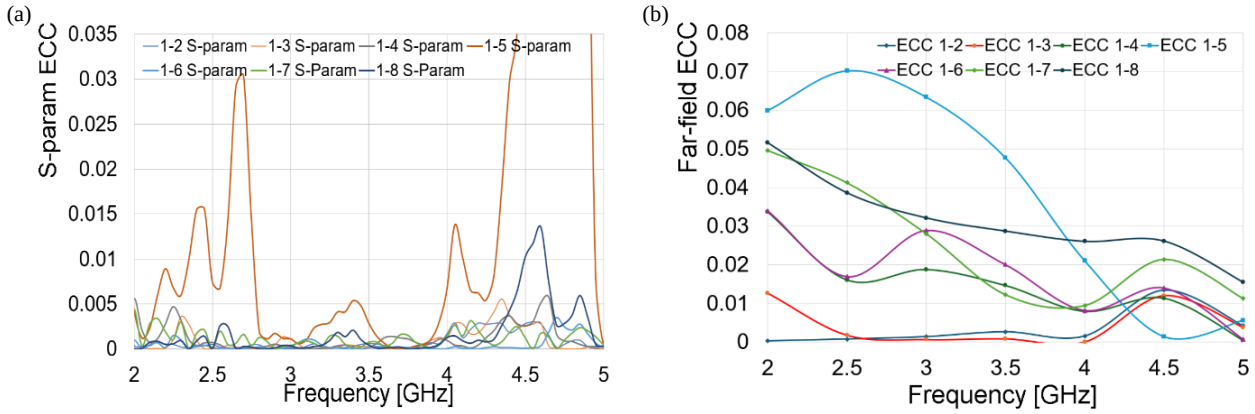

FIGURE 9. (a) Calculated *ECC* from measured S-parameters. (b) Calculated *ECC* from far-field.

flection response of individual antenna elements, are presented in Figure 8(a). Figure 8(b) shows the measured S_{i1} parameters, which quantify the isolation between different radiators in the array. As observed in Figure 8(a), each element exhibits good impedance matching at the design frequency. Additionally, the isolation between radiators, as indicated in Figure 8(b), is greater than 20 dB, reaching values even closer to 40 dB at 3.5 GHz.

To evaluate the overall efficiency of the antenna array, the measured Envelope Correlation Coefficient (*ECC*) metric is presented in Figure 9. This metric is calculated based on Equation (5).

Figure 9(a) depicts the (*ECC*) among Antenna 1 and the remaining antennas in the array using expression (5). This approach is justified by the symmetrical design of the array, which is expected to exhibit similar behavior for any chosen reference antenna; however, *ECC* can also be calculated using the relationship of the electric fields of the antennas under consideration. The far-field expression is given in (8).

$$\rho_{e_{ij}} = \frac{\left|\iint_{4\pi}\left[\vec{E}_i(\theta,\varphi)\cdot\vec{E}_j(\theta,\varphi)\right]d\Omega\right|^2}{\iint_{4\pi}\left|\vec{E}_i(\theta,\varphi)\right|^2 d\Omega \iint_{4\pi}\left|\vec{E}_j(\theta,\varphi)\right|^2 d\Omega} \tag{8}$$

where $\vec{E}_k(\theta,\varphi)$ is a complex vector function that describes the kth 3D radiation pattern at the Fraunhofer zone, $\cdot$ the Hermitian product, and $d\Omega$ the solid angle differential. The results considering (8) are presented in Figure 9(b). Comparing both figures, the behavior of the *ECC* obtained by the far-field method presents higher quantities, but still showing smaller values than 0.05 at the desired frequency of 3.5 GHz.

As evident in this figure, the *ECC* at the design frequency is significantly lower than 0.005, indicating a low level of correlation between the radiated fields from the antennas.

Figure 10 presents the measured Total Active Reflection Coefficient (*TARC*). To enhance clarity and avoid excessive curves, the *TARC* calculation adopted a similar strategy as the simulation process, setting all initial phases to zero, and in this case, varying θ_1 and θ_2. As observed in Figure 10, the measured *TARC* remains below -10 dB at the desired frequency. This result signifies that the system bandwidth is maintained between 3.4 GHz and 3.95 GHz, effectively covering the target frequency of 3.5 GHz, demonstrating that the array performance is not degraded by the interaction of multipath signals arriving with different phases.

Figure 11 presents the gain pattern for antenna number one. The Figure shows the co-polarization patterns in both H-plane and E-plane, along with the cross-polarization pattern in the H-plane. This result is consistent with the gain patterns observed for the remaining antennas in the array.

As observed in Figure 11, the antenna presents a quasi-omnidirectional gain pattern in the H-plane, while, in the E-plane, it shows a pair of nulls around 20° and 195°. On the

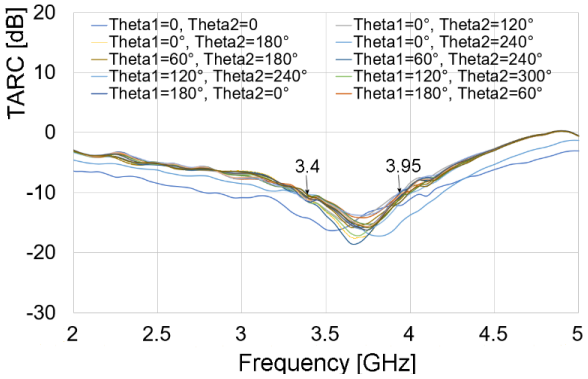

FIGURE 10. Measured *TARC* for different incoming signal phases.

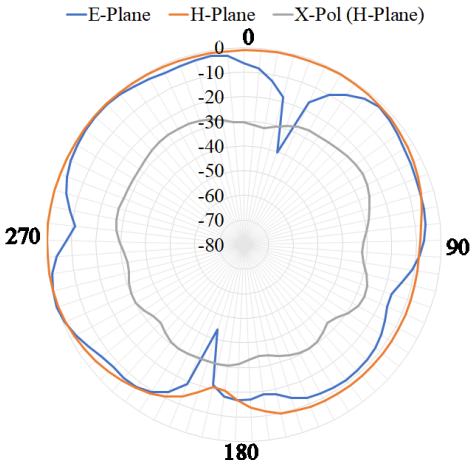

FIGURE 11. Normalized measured gain pattern of the Antenna 1 of the 8-element MIMO array.

TABLE 2. Antenna parameters at 3.5 GHz.

Peak directivity [dB]	Realized Peak gain [dB]	Radiation efficiency
-2.6	-2.03	0.994

TABLE 3. Comparison of 3-D MIMO antennas.

Reference	Bandwidth [GHz]	S_{ij} [dB]	*ECC*	*TARC* [dB]	Volume [mm^3]	X-pol [dB_copol]	Difficulty**
[14]	3.1–10.6	≤ -20	≤ 0.001	-11^*	$\sim 109,478$	~ 15	Complex
[15]	3.3–6.0	≤ -17	≤ 0.02	NA	$\sim 78,750$	NA	Medium
[16]	3.2–6.0	≤ -20	≤ 0.003	-10^*	$\sim 287,496$	NA	Medium
This work	3.25–3.95	≤ -20	≤ 0.05	-15	$\sim 91,125$	~ 30	Low

* Both [14] and [16] present only a single curve for the *TARC* parameter. However, to ensure good performance for MIMO applications, the *TARC* should be evaluated across various phase configurations [19]. As a result, [14] and [16] present an incomplete *TARC* analysis.

** The design complexity can be subjective, and this is just an appreciation of the authors, as different approaches with varying degrees of difficulty can achieve the desired goals. For instance, the antenna in [14] exhibits excellent ultra-wideband performance, but it necessitates a combination of a metamaterial Y-shaped structure and a π-shaped decoupling structure to achieve sufficient isolation between elements.

other hand, the cross-polarization level in the H-plane is lower than 30 dB compared to the co-polarization at the same plane. The measured gain of the antenna at 3.5 GHz is -2.3 dBi, a consequence due to the reduction of the overall size. However, the antenna is diminished more than 30% compared to a conventional disc monopole resonating at the same frequency, and the MIMO performance is excellent related to different structures given in the literature. Table 2 presents the antenna parameters report, which includes antenna realized peak gain, radiation efficiency, and peak directivity.

Finally, Table 3 presents a comparison of the present work to MIMO 3-D antennas. Regarding the Volume column, a regular body which fits each geometry was proposed, for example, this work was referenced to a cube of 45 mm sides.

In contrast, this work employs various phase configurations within the *TARC* equation, achieving an average value below -15 dB across all curves at the center frequency. This critical metric, absent in prior works, is essential for ensuring proper MIMO array function [19]. Consequently, a comparison of Table 2 reveals that the proposed design offers a well-balanced approach between performance and simplicity. It achieves good isolation, superior *TARC* values, comparable *ECC*, very low cross-polarization levels, compact size, and ease of design and fabrication.

5. CONCLUSIONS

This paper proposes an 8-port MIMO antenna utilizing a set of embedded Split Ring Resonators (SRRs). The SRR exhibits a double negative index metamaterial behavior at 3.5 GHz, enabling a compact element design compared to a conventional disc monopole. Consequently, the arrangement of the eight elements in orthogonal planes leads to a miniaturized array suitable for non-planar applications. This design eliminates the need for additional isolation techniques among radiators, as employed in some existing works, simplifying the design and fabrication process.

The proposed antenna achieves excellent MIMO performance metrics. The *TARC* parameter indicates a system bandwidth of approximately 900 MHz, a result not explicitly reported in other publications. The (*ECC*) exhibits values lower than 0.001, and the (*DG*) is around 20 dB. Finally, the cross-polarization level is approximately 30 dB lower than the co-polarization level.

ACKNOWLEDGEMENT

This work was supported by project SIP-IPN 202440839.

REFERENCES

[1] Tirado-Méndez, J. A., H. Jardón-Aguilar, F. Iturbide-Sánchez, I. Garcia-Ruiz, V. Molina-Lopez, and R. Acevo-Herrera, "A proposed defected microstrip structure (DMS) behavior for reducing rectangular patch antenna size," *Microwave and Optical Technology Letters*, Vol. 43, No. 6, 481–484, 2020.

[2] Li, W., D. Li, K. Zhou, Q. Fu, X. Yuan, and X. Zhu, "A survey of antenna miniaturization technology based on the new mechanism of acoustic excitation," *IEEE Transactions on Antennas and Propagation*, Vol. 71, No. 1, 263–274, 2023.

[3] Jardon-Aguilar, H., J. A. Tirado-Mendez, R. Flores-Leal, and R. Linares-Miranda, "Reduced log-periodic dipole antenna using a cylindrical-hat cover," *IET Microwaves, Antennas & Propagation*, Vol. 5, No. 14, 1697–1702, 2011.

[4] Tirado-Mendez, J. A., D. Martinez-Lara, H. Jardon-Aguilar, R. Flores-Leal, and E. A. Andrade-Gonzalez, "Inscribed fibonacci circle fractal in a circular radiator for ultra-wideband antenna operation and size reduction," *International Journal of Antennas and Propagation*, Vol. 2019, No. 1, 6393401, 2019.

[5] Li, M., K.-M. Luk, L. Ge, and K. Zhang, "Miniaturization of magnetoelectric dipole antenna by using metamaterial loading," *IEEE Transactions on Antennas and Propagation*, Vol. 64, No. 11, 4914–4918, 2016.

[6] Al-Saif, H., M. Usman, M. T. Chughtai, and J. Nasir, "Compact ultra-wide band MIMO antenna system for lower 5G bands," *Wireless Communications and Mobile Computing*, Vol. 2018, No. 1, 2396873, 2018.

[7] Wang, P., J. Liu, G. Huang, Q. Wu, C. Zhou, and W. Wang, "Wideband gain enhancement of high-isolation and quasi-omnidirectional metamaterial MIMO antenna for vehicular radar," *IEEE Transactions on Instrumentation and Measurement*, Vol. 71, 1–12, 2022.

[8] Shi, H., X. Zhang, J. Li, P. Jia, J. Chen, and A. Zhang, "3.6-GHz eight-antenna MIMO array for mobile terminal applications," *AEU — International Journal of Electronics and Communications*, Vol. 95, 342–348, 2018.

[9] Parchin, N. O., H. J. Basherlou, Y. I. A. Al-Yasir, and R. A. Abd-Alhameed, "A broadband multiple-input multiple-output loop antenna array for 5G cellular communications," *AEU — International Journal of Electronics and Communications*, Vol. 127, 153476, 2020.

[10] Mohanty, A. and B. R. Behera, "Design and analysis of compact 8-port dual-element MIMO antenna for wireless applications utilizing classical electromagnetic CMA approach," *AEU — International Journal of Electronics and Communications*, Vol. 145, 154077, 2022.

[11] Chen, W.-S., B.-Y. Lin, H.-T. Chen, and Y.-T. Liu, "Eight-port MIMO slot antennas for 5G C-band applications," in *2019 8th Asia-Pacific Conference on Antennas and Propagation (APCAP)*, 488–489, Incheon, Korea, 2019.

[12] Chen, Z., J. Huang, G. Dong, and G. Liu, "Dual-band 8-port 5G MIMO antenna," in *2021 International Conference on Microwave and Millimeter Wave Technology (ICMMT)*, 1–3, Nanjing, China, 2021.

[13] Jayant, S., G. Srivastava, and M. Khari, "8-port MIMO antenna having two notched bands for chipless UWB-RFID tags," *IEEE Journal of Radio Frequency Identification*, Vol. 6, 355–360, 2022.

[14] Shabbir, T., R. Saleem, S. S. Al-Bawri, M. F. Shafique, and M. T. Islam, "Eight-port metamaterial loaded UWB-MIMO antenna system for 3D system-in-package applications," *IEEE Access*, Vol. 8, 106 982–106 992, 2020.

[15] Huang, J., T. He, S. Xi, Q. Yang, X. Shi, and G. Liu, "Eight-port high-isolation antenna array for 3.3–6 GHz handset applications," *AEU — International Journal of Electronics and Communications*, Vol. 154, 154333, 2022.

[16] Kannappan, L., S. K. Palaniswamy, M. Kanagasabai, S. Kumar, R. T. Rao, and T. Govindan, "Sub-6 GHz eight-port 3-D vehicular antenna," in *2022 International Conference on Wireless Communications Signal Processing and Networking (WiSPNET)*, 293–296, Chennai, India, 2022.

[17] Jimenez-Guzman, G. A., J. A. Tirado-Mendez, and R. Pena-Rivero, "Small size antenna based on metamaterial split-ring resonators," *Microwave and Optical Technology Letters*, Vol. 55, No. 10, 2345–2350, 2013.

[18] Chen, X., T. M. Grzegorczyk, B.-I. Wu, J. Pacheco, Jr., and J. A. Kong, "Robust method to retrieve the constitutive effective parameters of metamaterials," *Physical Review E*, Vol. 70, No. 1, 016608, 2004.

[19] Fritz-Andrade, E., H. Jardon-Aguilar, and J. A. Tirado-Mendez, "The correct application of total active reflection coefficient to evaluate MIMO antenna systems and its generalization to N ports," *International Journal of RF and Microwave Computer-Aided Engineering*, Vol. 30, No. 4, e22113, 2020.